Title
Source and seed populations for relativistic electrons: Their roles in radiation belt changes

Permalink
https://escholarship.org/uc/item/3n1400k5

Journal
Journal of Geophysical Research: Space Physics, 120(9)

ISSN
2169-9380

Authors
Jaynes, AN
Baker, DN
Singer, HJ
et al.

Publication Date
2015-09-01

DOI
10.1002/2015JA021234

Peer reviewed

RESEARCH ARTICLE

Key Points:
- Source/seed energy electrons required to produce MeV radiation belt energization
- Substorm injections lead to VLF wave growth, producing MeV acceleration
- ULF waves may enhance loss/acceleration due to increased outward/inward diffusion

Correspondence to:
A. N. Jaynes,
allison.jaynes@lasp.colorado.edu

Source and seed populations for relativistic electrons: Their roles in radiation belt changes

A. N. Jaynes[1], D. N. Baker[1], H. J. Singer[2], J. V. Rodriguez[3,4], T. M. Loto'aniu[3,4], A. F. Ali[1], S. R. Elkington[1], X. Li[1], S. G. Kanekal[5], S. G. Claudepierre[6], J. F. Fennell[6], W. Li[7], R. M. Thorne[7], C. A. Kletzing[8], H. E. Spence[9], and G. D. Reeves[10]

[1]Laboratory for Atmospheric and Space Physics, University of Colorado Boulder, Boulder, Colorado, USA, [2]NOAA Space Weather Prediction Center, Boulder, Colorado, USA, [3]Cooperative Institute for Research in Environmental Sciences, University of Colorado Boulder, Boulder, Colorado, USA, [4]NOAA National Centers for Environmental Information, Boulder, Colorado, USA, [5]NASA Goddard Space Flight Center, Greenbelt, Maryland, USA, [6]Space Sciences Department, Aerospace Corporation, Los Angeles, California, USA, [7]Department of Atmospheric and Oceanic Sciences, University of California, Los Angeles, California, USA, [8]Department of Physics and Astronomy, University of Iowa, Iowa City, Iowa, USA, [9]Institute for Study of Earth, Oceans, and Space, University of New Hampshire, Durham, New Hampshire, USA, [10]Space Science and Applications Group, Los Alamos National Laboratory, Los Alamos, New Mexico, USA

Abstract Strong enhancements of outer Van Allen belt electrons have been shown to have a clear dependence on solar wind speed and on the duration of southward interplanetary magnetic field. However, individual case study analyses also have demonstrated that many geomagnetic storms produce little in the way of outer belt enhancements and, in fact, may produce substantial losses of relativistic electrons. In this study, focused upon a key period in August–September 2014, we use GOES geostationary orbit electron flux data and Van Allen Probes particle and fields data to study the process of radiation belt electron acceleration. One particular interval, 13–22 September, initiated by a short-lived geomagnetic storm and characterized by a long period of primarily northward interplanetary magnetic field (IMF), showed strong depletion of relativistic electrons (including an unprecedented observation of long-lasting depletion at geostationary orbit) while an immediately preceding, and another immediately subsequent, storm showed strong radiation belt enhancement. We demonstrate with these data that two distinct electron populations resulting from magnetospheric substorm activity are crucial elements in the ultimate acceleration of highly relativistic electrons in the outer belt: the source population (tens of keV) that give rise to VLF wave growth and the seed population (hundreds of keV) that are, in turn, accelerated through VLF wave interactions to much higher energies. ULF waves may also play a role by either inhibiting or enhancing this process through radial diffusion effects. If any components of the inner magnetospheric accelerator happen to be absent, the relativistic radiation belt enhancement fails to materialize.

1. Introduction

Early studies of high-energy electrons at geostationary orbit (L ~ 6.6) showed a clear relationship between episodes of high-speed solar wind and subsequent relativistic electron enhancements [*Paulikas and Blake*, 1979; *Baker et al.*, 1979]. This led to the view that magnetospheric substorm activity driven by high solar wind speed played a key role in providing "seed" electrons of energy up to a few hundred keV in kinetic energy [*Baker et al.*, 1986]. Studies based upon data from the Solar, Anomalous, and Magnetospheric Particle Explorer and Polar missions also showed that high-speed solar wind streams were effective at producing outer radiation belt electron flux enhancements [*Baker et al.*, 1997; *Kanekal et al.*, 1999]. Using data from the Highly Elliptical Orbit spacecraft, it was also shown that for strong relativistic electron acceleration to occur throughout the entire outer zone, the solar wind was required to have southward interplanetary magnetic field (IMF) directionality [*Blake et al.*, 1997].

Studies related to this early work demonstrated on a statistical basis that many geomagnetic storms produced relativistic electron flux enhancements at GEO (geostationary orbit), but many other storms did not [*Summers et al.*, 2004; *Hudson et al.*, 2008]. *Reeves et al.* [2003] specifically showed that ~50% of storms over a several year period exhibited a high-energy electron flux increase while ~25% showed an actual flux decrease during strong storm activity. The remaining 25% of cases showed essentially no flux change

between the prestorm levels and the poststorm levels. Studies of the "total radiation belt content" [*Baker et al.*, 2004] and a more extended study of GEO flux relations to solar wind drivers [*Reeves et al.*, 2011] found that the relativistic electron-solar wind speed relationship is not a simple linear one. For example, *Reeves et al.* [2011] found that a scatterplot of electron flux and solar wind speed formed a "triangle" with a speed-dependent lower limit to fluxes but a speed-independent upper limit. Further analysis of the same data set [*Li et al.*, 2011] compared 15 years of solar wind data to GEO observations of MeV electron flux and found that high solar wind speeds are not necessary for MeV enhancements; instead, southward IMF is the essential condition to cause acceleration of MeV electrons in the outer radiation belt.

The Van Allen Probes pair of NASA spacecraft were launched on 30 August 2012. These spacecraft have ideal instruments to measure the relativistic electron component throughout the Van Allen zones. The Relativistic Electron-Proton Telescope (REPT) investigation [*Baker et al.*, 2012] measures ~1 to 20 MeV electrons. The Van Allen Probes also have the Magnetic Electron-Ion Spectrometer (MagEIS) investigation [*Blake et al.*, 2013] to measure low- and medium-energy (~30 keV to ~1 MeV) electrons and complete wave data from the Electric and Magnetic Field Instrument Suite and Integrated Science (EMFISIS) experiment [*Kletzing et al.*, 2013]. Together, the overall Van Allen Probes payload has given an unprecedented view of the acceleration, transport, and loss of radiation belt particles.

Early results from the Van Allen Probes mission revealed unexpected morphological features of the Van Allen belts such as a transient third belt or "storage ring" feature [*Baker et al.*, 2013]. This previously unreported aspect of the outer trapping region has been studied in detail theoretically [*Thorne et al.*, 2013a] and had been previously observed only in proton data [*Hudson et al.*, 1997], not electron populations. Another surprising structural feature of the ultrarelativistic electron distribution is the extremely sharp inner edge of the outer zone at L = 2.8 [*Baker et al.*, 2014a]. This work has clearly shown that very strong spatial gradients can persist for long periods in high-energy electron radiation belt distributions. Consequently, the inner zone is shielded from inward radial diffusion and is largely devoid of electrons at energies $E \gtrsim 1$ MeV [*Baker et al.*, 2014a; *Li et al.*, 2015; *Fennell et al.*, 2015].

Detailed studies of specific events using the dual Van Allen Probes have shown the way in which strong geomagnetic storms can accelerate electrons to relativistic energies. *Reeves et al.* [2013] studied a powerful storm in October 2012 that exhibited "local" acceleration due to chorus wave interactions with seed electrons at $L \sim 4.2$. This was modeled by *Thorne et al.* [2013b] to show very good quantitative understanding of the wave-particle acceleration mechanism. *Baker et al.* [2014b] studied a period in March 2013 that exhibited both a relatively gradual acceleration event due to a high-speed solar wind stream as well as a separate, very abrupt local acceleration event driven by impact of a strong solar coronal mass ejection (CME). *Foster et al.* [2014] in a companion paper to *Baker et al.*'s [2014b] study showed that an intense magnetospheric substorm event played a key and central role in the abrupt relativistic electron acceleration event in March 2013. Again, this particular event occurred deep within the outer radiation belt associated with chorus-wave interactions as in the *Reeves et al.* [2013] event.

Based on the already extensive studies of outer zone electron acceleration from the Van Allen Probes mission, we have been curious to examine cases where elements of the overall acceleration scenario were missing. An ideal situation presented itself when observations from the Geostationary Operational Environmental Satellite (GOES) spacecraft [*Onsager et al.*, 1996; *Singer et al.*, 1996] showed an extended, and rather unexpected, anticorrelation of solar wind speed with GEO relativistic electron fluxes. This period in September 2014 is the focus of our detailed, multisatellite study reported here.

2. Electron Local "Heating" Acceleration Mechanism

While earlier studies have previously implied this mechanism [e.g., *Green and Kivelson*, 2004; *Chen et al.*, 2006], several recent studies have documented the indisputable occurrence of localized acceleration of energetic electrons to multi-MeV energies deep within the outer radiation belt ($3.5 \lesssim L \lesssim 5.0$). These studies [*Reeves et al.*, 2013; *Baker et al.*, 2014b; *Foster et al.*, 2014] have been bolstered by theoretical modeling [e.g., *Thorne et al.*, 2013b; *Li et al.*, 2014; *Tu et al.*, 2014] to show that low-energy (few to tens of keV) electrons can fuel the growth of chorus waves that, in turn, can act on even more energetic (tens to hundreds of keV) substorm-injected electrons to produce relativistic electrons in the outer zone. This mechanism can operate on quite short time scales.
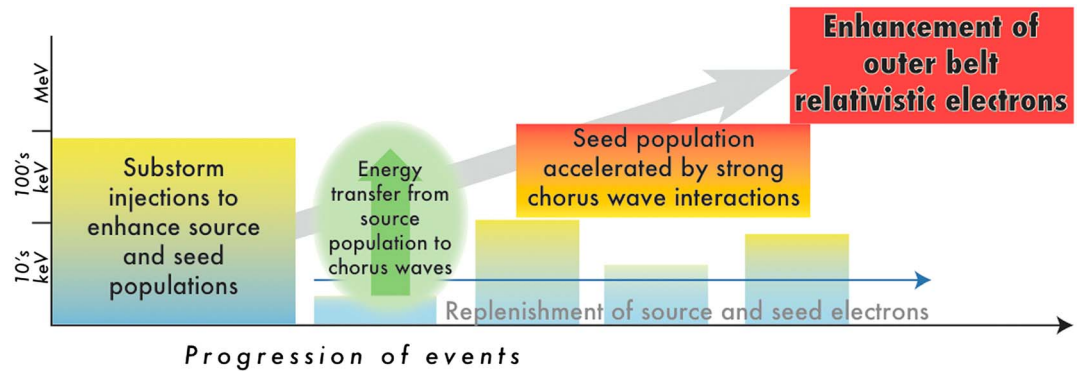
Figure 1. Schematic of the ideal setup and sequence for strong enhancement of outer belt electrons >1 MeV.

Figure 1 shows a schematic diagram of the key ingredients of the local acceleration mechanism. An isolated event exhibiting this local heating process normally begins with a strong solar wind forcing event: This typically would be a strong southward turning of the IMF which then loads substantial energy into the Earth's magnetotail. This in turn leads to a strong magnetospheric substorm onset after about a 1 h long growth phase [*McPherron et al.*, 1973]. The substorm onset almost invariably is accompanied by an injection of low- to medium-energy electrons into the Earth's inner magnetosphere [e.g., *Baker et al.*, 1996, and references therein]. We generally describe the hot plasma (~1 keV) and lower energy energetic electrons (tens of keV) in substorm events as the "source" population of particles. As discussed by *Thorne et al.* [2013b, and references therein], this source population of electrons has anisotropic angular distributions that feed free energy into electromagnetic waves in the lower chorus band. Such chorus waves can, in turn, interact resonantly with higher energy (30–300 keV) electrons also injected by substorms. We call these medium-energy electrons the seed population of particles. Chorus waves Doppler shifted to the cyclotron frequency of the seed population electrons can very efficiently heat (and accelerate) such electrons to multi-MeV energies through resonant interactions [e.g., *Boyd et al.*, 2014]. As shown in Figure 1, substorms are necessary to produce the initial energetic electron population. Thereafter, amplified chorus waves transfer energy from the source electrons to a portion of the seed electrons. These seed electrons can be pumped up in energy by large factors on characteristic time scales of minutes to hours [*Summers et al.*, 2002; *Horne et al.*, 2005; *Thorne et al.*, 2013b; *Summers et al.*, 2012].

A question we wish to address in the present paper is what happens if key elements of the acceleration mechanism portrayed in Figure 1 are absent altogether or are taken away at some point in an acceleration sequence? Can we use geostationary orbit, Van Allen Probes, and other data to look at weak or interrupted acceleration events when key steps in the progression do not materialize? Examining such alternative scenarios helps us gain a deeper understanding of how the "normal" acceleration events really work.

3. August–September 2014 Event Overview

Our first recognition of an unusual and quite long-lasting depletion of relativistic electrons in the outer radiation belt came from the real-time operational GOES data at geostationary orbit. Figure 2 provides in the top plots a long run of GOES 13 Magnetospheric Electron Detector data [*Hanser*, 2011] for the period 1 August 2014 to 15 October 2014 from Telescope 5 whose center pitch angle is close to 90° during most of the period. The lowest energy channel (plotted as the black trace in Figure 2) is for 30 to 50 keV electrons. The GOES 13 $E > 2.0$ MeV electron fluxes, used by the NOAA Space Weather Prediction Center for its real-time alerts when the flux exceeds 1000 cm^{-2} s^{-1} sr^{-1}, are shown by the purple colored trace in Figure 2. The light brown coloration associated with the $E > 2.0$ MeV measurements in the figure is for times when the background rate in that channel was greater than 30% of the observed total count rate. The background level in the $E > 2.0$ MeV electron channel is estimated using the empirical expression used by Space Weather Prediction Center in its real-time processing of this channel, which consists of a linear combination of the fluxes from four GOES solar proton channels between 8.7 and 200 MeV. For details please refer to *Rodriguez* [2014]. During most of the period shown in Figure 2, the backgrounds were due to the slowly varying galactic cosmic ray flux, the exception being 11–13 September, when a weak solar energetic particle (SEP) event occurred. During this period, GOES 13 is at local midnight at approximately 05:00 UT.
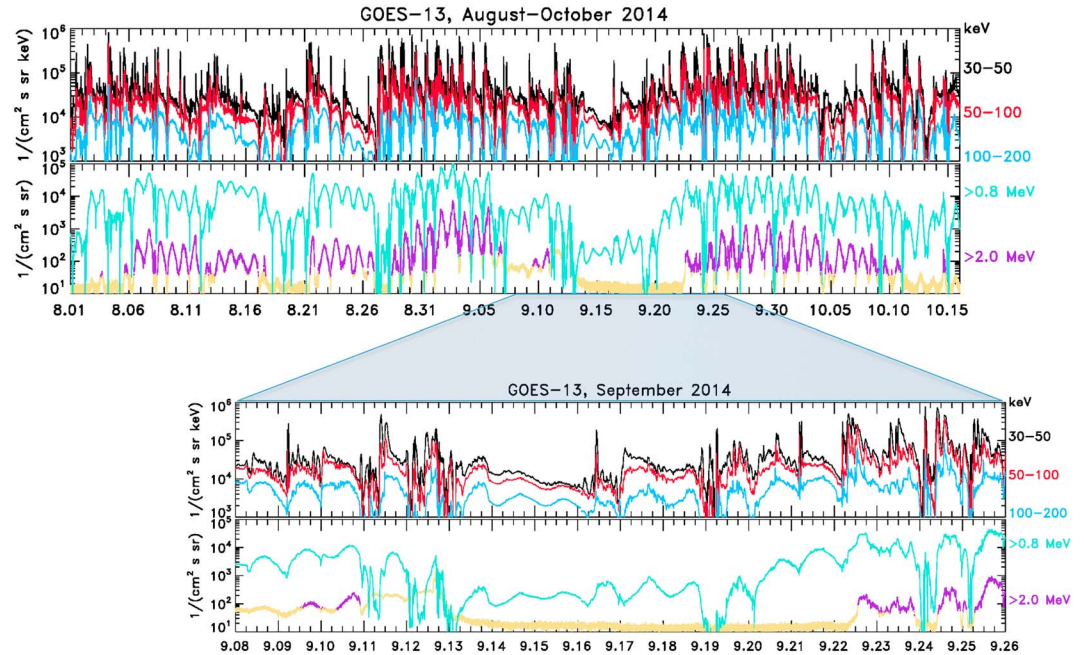
Figure 2. Overview of GOES observations over range of energies: 1 August to 15 October, and 8–26 September for inset. Light brown traces indicate the fluxes for times when the background count rate is at least 30% of the observed count rate. Days 11–13 of September is during a weak SEP event, and 13–22 September is when the >2 MeV electrons are below the galactic cosmic ray instrument backgrounds.

A striking diminution of $E > 2.0$ MeV electrons below the background level was observed during the period 13 September to 22 September 2014. Such reductions at geostationary orbit, usually of shorter duration than this case, have been reported previously and have been studied extensively [*Onsager et al.*, 2002, 2007; *Green et al.*, 2004]. However, to our knowledge such a deep and long-lasting decrease of relativistic electrons at GEO as this one has not been reported previously. During the entire period shown in Figure 2, the north-south component of the GOES 13 magnetic field (not shown) was positive, indicating that the GOES 13 spacecraft was located inside the magnetopause [*Rufenach et al.*, 1989], while the $E > 2$ MeV electron fluxes were below background levels during 13–22 September. Therefore, the observations show that the trapped $E > 2$ MeV electron population in the magnetosphere—at least near GEO—was greatly depleted and was below GOES instrument background levels for nearly 10 days.

In the lower portion of Figure 2 we show an expanded view of the GOES 13 data for the period 8 September through 25 September 2014. These data demonstrate that electrons in the lower energy ranges (30–200 keV) also were quite reduced in flux levels beginning on 13 September and extending to 16 September. Not until the middle of 16 September did one see a return to the pattern of spikey bursts of these medium-energy electrons. Such bursts are closely associated with substorm injection events [*Baker et al.*, 1996; *Sergeev et al.*, 2015]. From the long run of data shown in Figure 2, we would conclude that the period from 13 to 22 September was remarkably devoid of $E > 2$ MeV electrons and was also quite reduced in the flux and occurrence frequency of substorm-injected medium-energy seed electrons.

The solar wind, IMF, and geomagnetic conditions as they relate to the geostationary orbit electron flux data just described are shown in Figure 3. The top plot presents the auroral electrojet (*AE*) index, the geomagnetic storm (*Dst*) index, the solar wind dynamic pressure (*P*), the IMF north–south (B_z) component, and the solar wind speed (*V*) for the period 25 August to 4 October 2014. The lower portion of Figure 3 shows these same quantities on an expanded time scale for 8-26 September.

A dominant feature of the data portrayed in Figure 3 is the high-speed solar wind stream that was observed beginning on 12 September and lasting until ~16 September. The peak solar wind speed was >700 km/s and the speed remained relatively high (≳500 km/s) for several days. Based on research cited previously [e.g., *Baker et al.*, 1986, 1997a] we would have expected this stream to produce a large, long-lasting enhancement of relativistic electrons at GEO; instead (as shown in Figure 2) the $E > 2$ MeV fluxes were quite depleted.
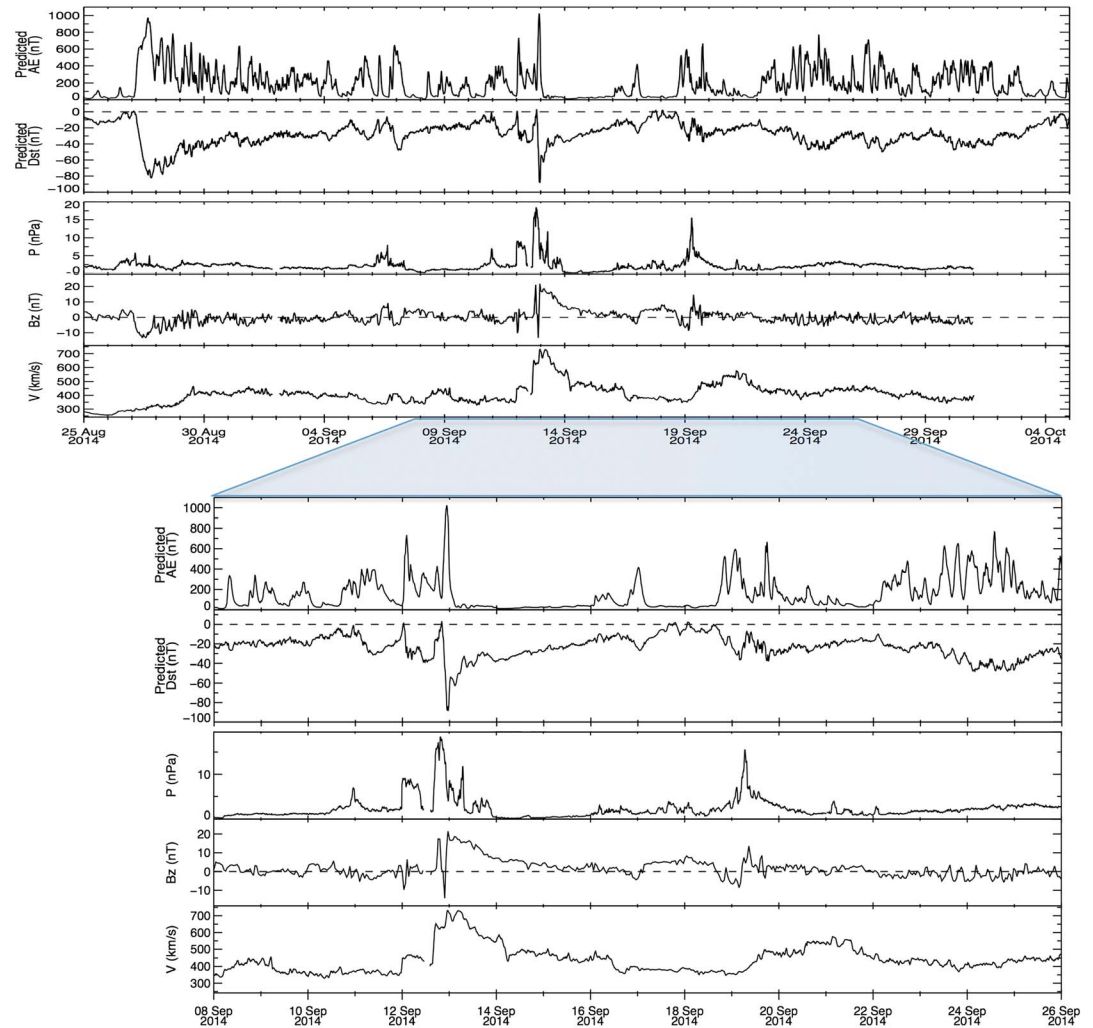
Figure 3. Predicted *AE* [*Luo et al.*, 2013] and *Dst* [*Temerin and Li*, 2006], with solar wind pressure, B_z and velocity: 25 August to 4 October, and 8–26 September for inset.

Other features of the solar wind and geomagnetic drivers for this period are interesting as well. Note in Figure 3 that the leading edge of the high-speed solar wind stream was accompanied by high dynamic solar wind pressure (reaching nearly 20 nPa late on 12 September), potentially indicating a CME (coronal mass ejection) embedded within the high speed stream. The north-south component of the GOES 15 magnetic field (not shown) went strongly negative between 22:18 and 22:23 UT on 12 September when the satellite was ~1.5 h past local noon, indicating that the magnetopause was briefly pushed inward of geostationary orbit [*Rufenach et al.*, 1989]. The increased solar wind speed and dynamic pressure drove strong geomagnetic activity ($AE \sim 1000$ nT and $Dst \sim -90$ nT) at that same time. However, abruptly after this peak of geomagnetic activity, the IMF turned strongly northward and it remained so for over a day. In fact, the IMF remained at least weakly northward for most of the period 13–21 September. This prolonged northward IMF—especially on 13–15 September—reduced the *AE* level to virtually zero. This absence of substorm activity explains the absence of seed population injections witnessed in the GOES 13 data (Figure 2) as discussed above and, most likely, the absence of source population electrons as well.

The period 13 September to roughly 20 September contrasts strikingly with periods preceding (27 August to 7 September) and succeeding (22 September to 2 October) the interval of our central attention. Both of these other "bracketing" time intervals had high, almost continuously fluctuating levels of geomagnetic activity (as measured by the *AE* index). In fact, both of these adjacent periods are quite similar to the pattern
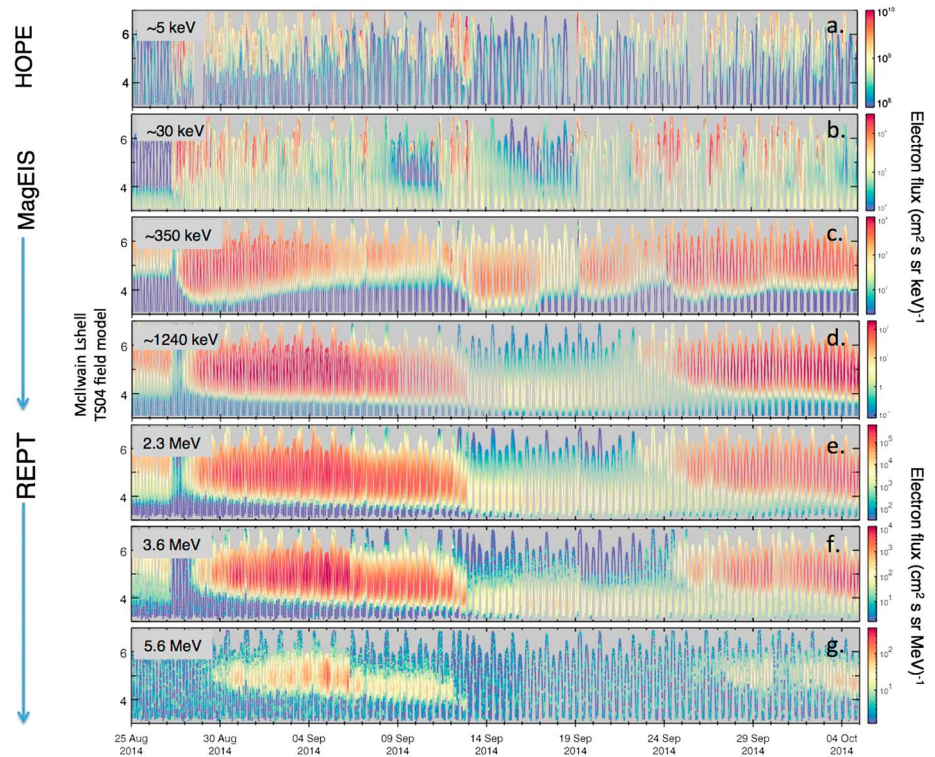
Figure 4. Spin-averaged flux over HOPE, MagEIS and REPT energy range: 25 August to 4 October.

termed "high-intensity, long-duration, continuous *AE* activity" (HILDCAA) intervals [*Tsurutani et al.*, 1995]. As noted in recent studies [*Miyoshi and Kataoka*, 2008; *Hajra et al.*, 2015], HILDCAA events can often be quite effective at producing high-energy electrons at geostationary orbit. This is well borne out by examination of the GOES 13 data in Figure 2 and by comparing those data with the *AE* and IMF records in Figure 3. Additionally, in Figure 4, the 27 August event appears to be a particularly well-behaved acceleration event, with source energy electrons appearing prior to seed and MeV populations, and sustaining high fluxes well into the buildup of the MeV belt.

A broader view of energetic electron properties throughout the outer radiation belt is shown in Figure 4 based on Van Allen Probes measurements. This multipanel plot shows color-coded intensities of electrons in various selected energy ranges from ~5 keV (top) to 5.6 MeV (bottom) for the period 25 August through 4 October 2014, from the Van Allen Probes Radiation Belt Storm Probes Energetic Particle, Composition, and Thermal Plasma (RBSP-ECT) instrument suite [*Spence et al.*, 2013]. The top plot is from the Helium, Oxygen, Proton, and Electron (HOPE) experiment [*Funsten et al.*, 2013], the next three panels are from the MagEIS experiment [*Blake et al.*, 2013], and the lower three panels are from the REPT experiment [*Baker et al.*, 2013]. The data are portrayed as a function of [*McIlwain*, 1966] L parameter (vertical axis) and time (horizontal axis) for each energy range. During this period, the apogee of the Van Allen Probes was located near 5.5 magnetic local time (MLT), and the local time coverage above L = 4.0 encompassed the dawn sector covering ~1.5–8.5 MLT.

As is evident from Figure 4, electrons from a few keV to several MeV were all concurrently depleted early on 27 August at the beginning of the *Dst* and *AE* enhancement on that date (see Figure 3). Thereafter, progressively higher and higher energy particles built up in flux throughout the days of 27 August and 28 August. This enhancement of electron intensity occurred from L ~ 3.5 out to the edge of the radiation belt sampled by Van Allen Probes (L ≳ 6.5). High-energy electron flux enhancement persisted until 13 September. As was noted above, the electron enhancement seen throughout most of the outer zone from 27 August to ~7 September was closely associated with the HILDCAA-like period identified in the simultaneous *AE* and IMF data (Figure 3).
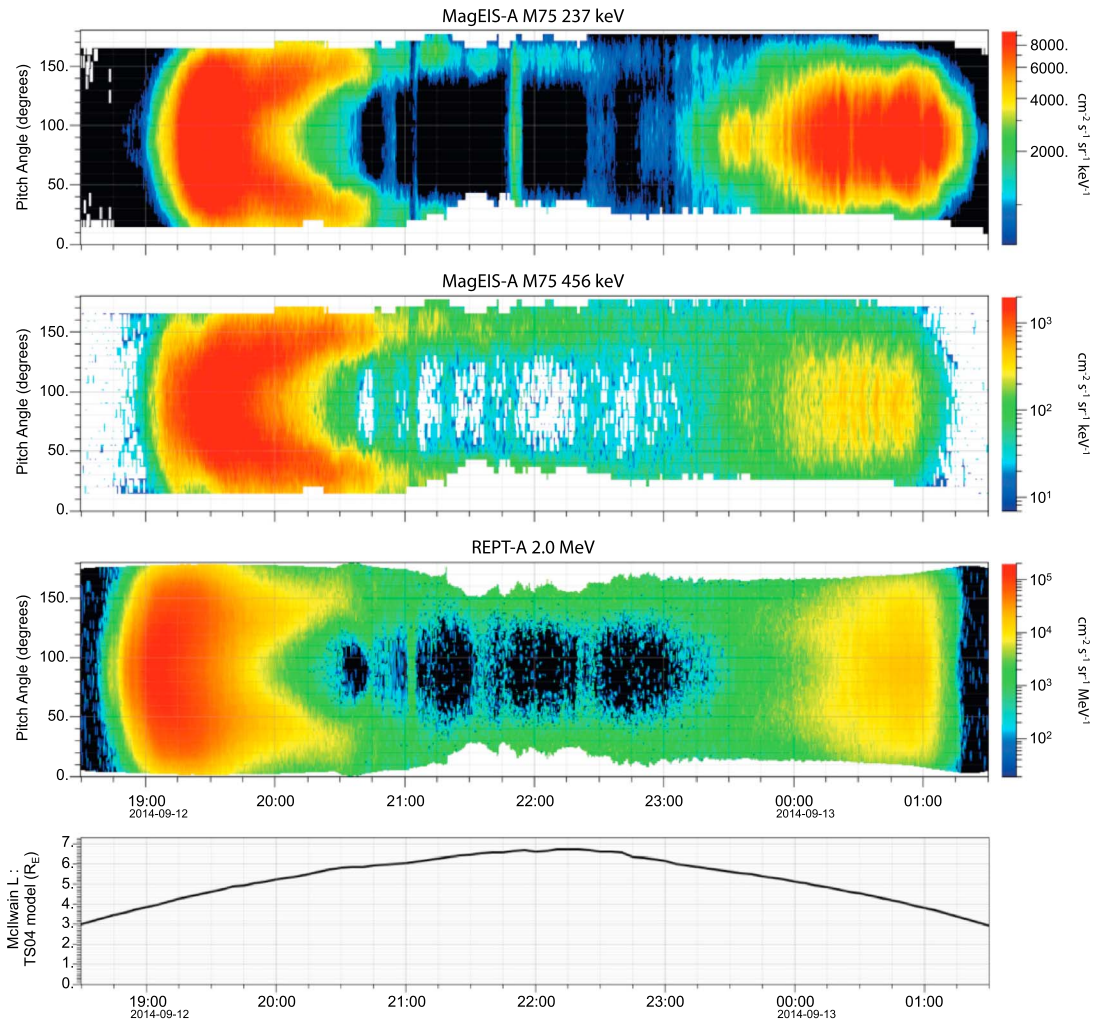
Figure 5. Pitch angle distribution spectrograms for selected (top) REPT and MagEIS energies for the period of magnetopause shadowing loss during the main phase of the 12 September storm and (bottom) McIlwain L-shell value calculated in the TS04 magnetic field model.

Given the strong solar wind speed increase on 12 September, we would have expected a large further relativistic electron flux increase on 13 September and the days following. Instead, the fluxes measured by the Van Allen Probes at energies from ~1 MeV to at least 7 MeV were seen to have been strongly depleted. This depletion lasted from the beginning of 13 September to 22–24 September (depending on particle energy). The flux reduction seen by the Van Allen Probes sensors comports very well with the flux reduction interval also seen by GOES 13 (see Figure 2) as described previously.

From Figure 4 it is seen that the ~5 keV and ~30 keV electrons were diminished over essentially all L shells (Figures 4a and 4b) on 13 September and largely remained so until ~19 September. This is indicative of the source electron population being substantially reduced in association with the dropout of relativistic electrons. On the other hand—and somewhat curiously—the ~350 keV electrons (Figure 4c) appear to be rapidly transported deeper into the outer zone over the period 12 September into 13 September, meaning that the seed population was actually enhanced during the period 13–16 September (at least for $3.0 \leq L \leq 4.5$). Short-lived depletions for ~350 keV at 90° pitch angles are evident just after the storm main phase (Figure 5), although they are quickly built up to prestorm levels within hours. Thus, it can be the case that source electrons and relativistic electrons can be depleted in the long term even while seed electrons get (at least locally) enhanced. The distinctly different behavior between the 350 keV (seed) electrons and those at higher (>MeV) energy is probably related to the prevailing radial phase space density (PSD) gradient. Electrons with magnetic moment below a few hundred MeV/G have a positive
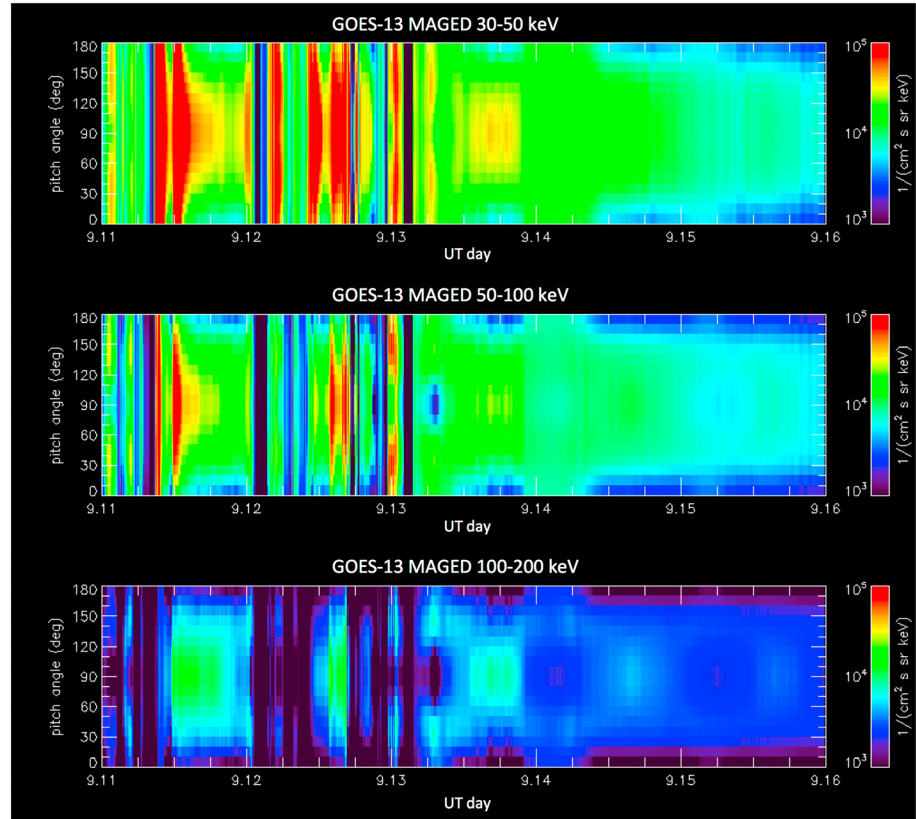
Figure 6. Pitch angle distribution spectrograms for selected GOES 13 energies: 11–15 September.

radial gradient, while those with higher magnetic moment develop peaks near L~ 4–4.5 associated with local acceleration during the previous magnetic storm. As demonstrated later in section 5, during the period around September 13 there was a considerable increase in ULF wave activity, which would rapidly drive lower energy electrons inward and lead to enhanced flux at lower L as observed. The increase in radial diffusion would also drive relativistic electrons outside the PSD peak toward the magnetopause boundary where they would be lost by magnetopause shadowing. Removal of the relativistic population inside the PSD peak may require another mechanism such as loss to the atmosphere by EMIC scattering, but confirmation of this will require detailed quantitative modeling.

Note in Figure 4 that on 22 September to late 24 September (depending on electron energy), the relativistic electron populations were substantially restored to high-intensity levels. This restoration corresponded to a clear period of strong *AE* activity and, hence, to further HILDCAA-like behavior. High electron fluxes continued to be seen until ~4 October in association with the elevated *AE* and solar wind activity. Comparing Figure 2 with Figure 4, we again note that the electron behavior for the broad range of L values sampled by the Van Allen Probes instruments comports well with the electron fluxes measured at the more limited L range sampled by GOES 13.

4. Detailed Examination of the 12–24 September Depletion Event

The rapid decrease of radiation belt electrons late on 12 September shown in Figure 4 is quite distinctive. The decrease was observed at energies of a few keV as well as from ~1 MeV up to the multi-MeV range. In Figure 5 we show pitch angle versus time plots, color-coded by flux intensity, for several selected Van Allen Probes energy channels. We see that beginning at ~19:50 UT on 12 September and for the next several hours, the electrons measured by sensors on the RBSP-A spacecraft showed strong minima at 90° pitch angles at L > 6. This is consistent with the magnetopause "shadowing" mechanism [e.g., *Wilken et al.*, 1982; *Turner et al.*, 2012; *Hietala et al.*, 2014] and suggests that the radiation belt depletion was caused by particles being lost through the dayside magnetospheric boundary. This picture is supported by two pieces of evidence: (1) the *Shue et al.* [1998] model gives a magnetopause standoff distance close to GEO for several
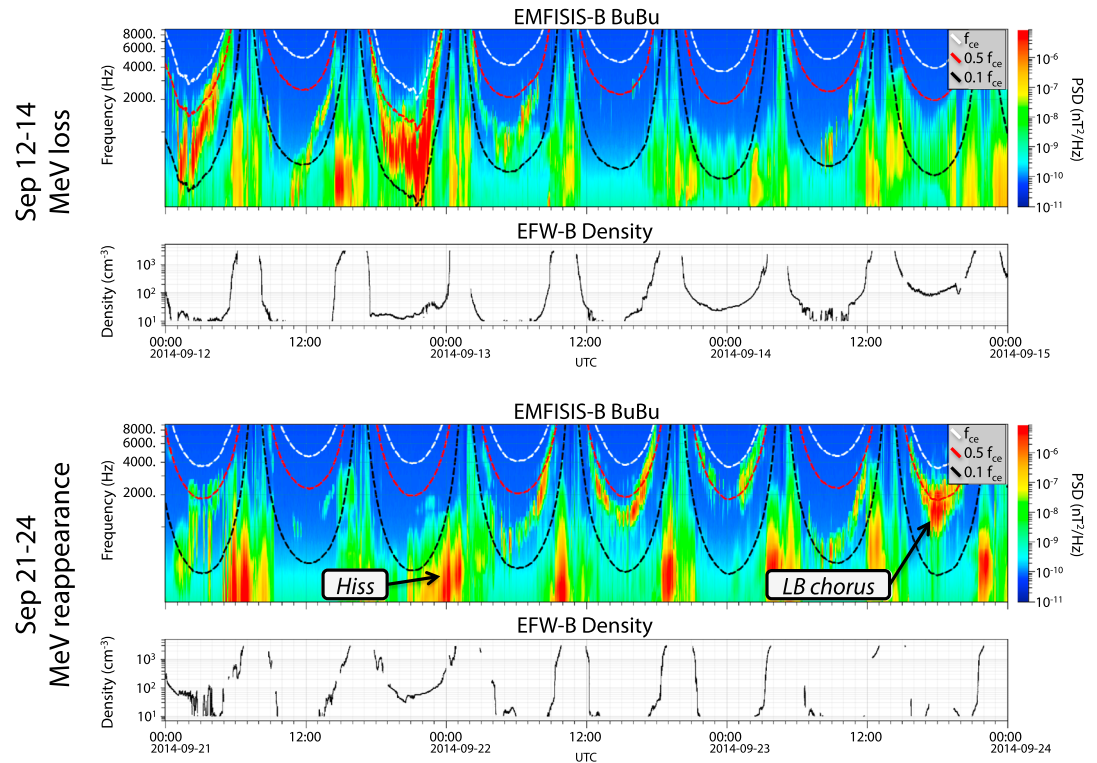
Figure 7. Chorus wave power spectral density spectrograms from EMFISIS-B magnetic field measurements and electron density derived from spacecraft potential during the (top) 12 September storm and (bottom) recovery of relativistic outer belt; lines denote fractions of the electron gyrofrequency at 0.1 f_{ce} (black), 0.5 f_{ce} (red), and 1.0 f_{ce} (white) in order to bound the lower and upper band chorus observations.

hours during the depletion event and (2) the enhancement in ULF wave power during this time is sufficient to drive this process (discussed further in the next section). As expected, similar pitch angle distributions for GOES 13 [*Hartley et al.*, 2013] in the 30–200 keV electron energy range (Figure 6) also show such depletions in the 90° pitch angle range. Notably, this figure demonstrates that overall electron intensities at GEO in this energy range were much reduced from 13 September onward.

5. Observed Wave Activity

From the scenario portrayed in Figure 1, we would expect that an absence of substorm activity on 13 September and on subsequent days would mean that the source populations of electrons would be quite reduced. Without ample source electrons to supply free energy, the chorus wave activity should diminish greatly as well. Figure 7 shows EMFISIS wave data for 12–14 September and for 21–23 September. The top plots for the time of radiation belt depletion (late on 12 September into 13 September) show that lower band chorus went away almost completely on 13 and 14 September in the vicinity of the Van Allen Probes. This remained largely the case (data not shown here) until 22 September when the lower band chorus reemerged (see bottom plots in Figure 7).

A more global indicator of chorus wave activity comes from Polar-Orbiting Operational Environmental Satellite (POES) data. This recently developed technique [*Li et al.*, 2013] uses POES electron precipitation data over 30–100 keV to infer chorus wave intensity. Figure 8 shows that, indeed, chorus wave activity was strong until late on 12 September and early on 13 September. Wave activity then was minimal at all MLT sectors from later on 13 September through 18 September. A brief episode of chorus enhancement occurred on 19–21 September, but strong chorus resurgence did not occur until 22 September. This is when GOES saw a return of substorm electron injections (Figure 2) and when the *AE* index again became enhanced (see Figure 3). These injections and enhanced *AE* activity occurred after the fluctuating B_z component of the IMF turned weakly southward at approximately 02:00 UT on 22 September, never decreasing below −5 nT for the rest of the day.
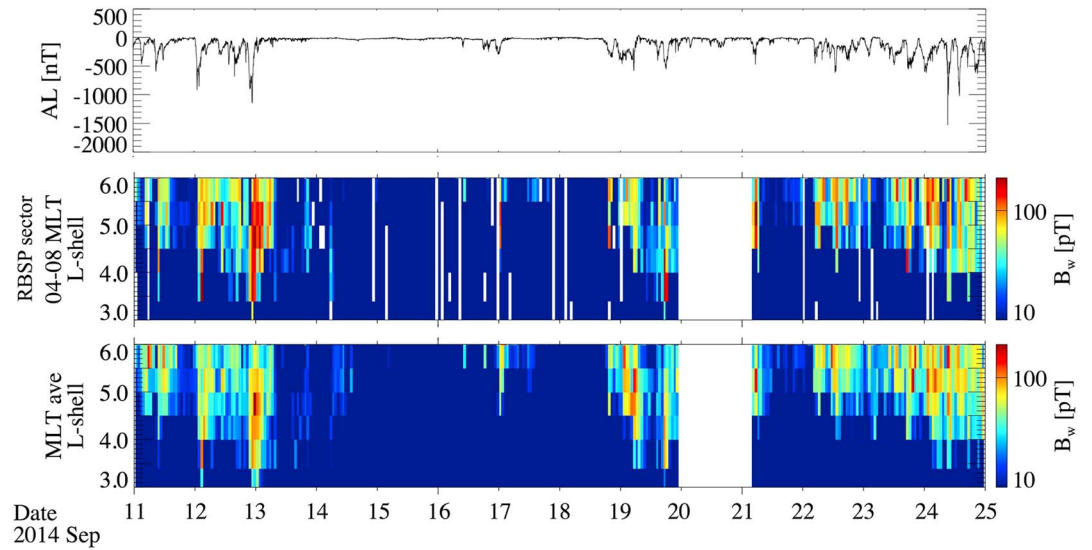
Figure 8. Inferred chorus wave amplitudes by using a proxy based on POES electron precipitation measurements (30–100 keV). (top) *AL* index. (middle) Evolution of inferred chorus wave amplitude averaged over 04:00–08:00 MLT, where the apogees of the Van Allen Probes were located. (bottom) Evolution of inferred chorus wave amplitude averaged over all MLTs.

The contribution to this process as a whole by ultralow frequency (ULF) waves is likely an enhancement or suppression of individual episodes in the normal sequence depending on the phase space density gradient and the magnetopause location. Figure 9 shows an overview of the Pc5 ULF power in the compressional component as observed in situ by the Van Allen Probes' EMFISIS fluxgate magnetometers. The figure indicates that both spacecraft saw almost identical ULF wave activity that can be summarized as follows. The Pc5 power was enhanced during the main phase of the 12 September storm and lasted through 13 September before settling at prestorm levels. The power spectral density peak occurs at approximately 5–6 mHz over the orbit of enhanced power from 12 to 13 September. At this frequency, for a drift resonance condition given as $\omega_{\text{wave}} = m_{\text{wave}}\omega_{\text{drift}}$ and assuming $m = 1$, we expect resonance for
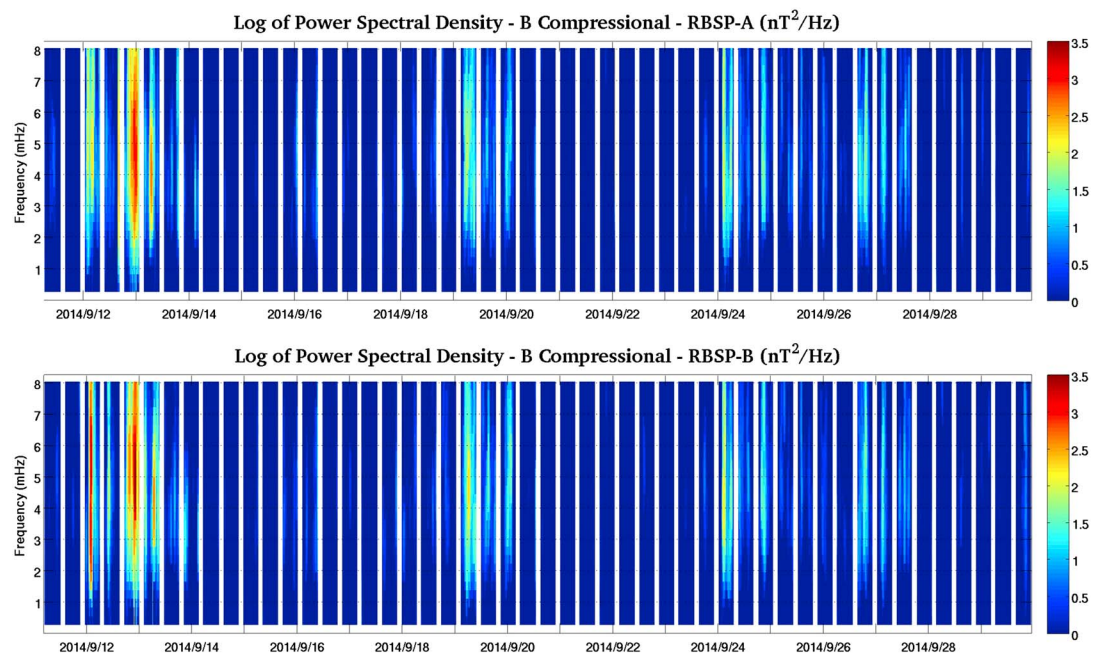

Figure 9. ULF power spectral density overview during the September storm through to the recovery of the MeV: 11–30 September.

electrons with energies of 5 MeV to >8 MeV. However, with higher mode numbers, the resonant energy can decrease to as low as 100s of keV. Indeed, a distribution of mode numbers is possible up to $m > 15$, particularly during times of high-speed solar wind [*Elkington et al.*, 2012; *Claudepierre et al.*, 2008]. Thus, ULF waves may have played a direct role in the disappearance of the outer belt on 13 September by driving outward radial diffusion from multi-MeV energies down to seed population energies.

ULF power is again enhanced following 24 September, during the reappearance of the MeV outer belt. Similarly to the previous episode, the observed ULF peak frequencies would most readily resonate with multi-MeV to 100s of keV electrons. ULF waves may be partly responsible for the rebuilding of the outer belt after 24 September. However, the chorus waves reappear at an earlier time, on 22 September, as the Van Allen Probes start to observe acceleration occurring over a wide energy range. Until a deeper analysis is performed, the effect of the enhanced ULF wave power on the particle energization or inward diffusion is not immediately straightforward.

6. Spectral Changes During Storm Times

Early work at GEO [e.g., *Baker et al.*, 1986] suggested that energetic electron spectra could be adequately approximated as simple power law distributions. During the period of high solar wind speed and strong substorm activity, it was inferred that a steep power law was appropriate. This meant there were copious quantities of lower energy (source and seed) electrons, while on the trailing edge of high-speed streams the spectrum was much harder with large relative enhancement of electrons in the MeV and multi-MeV range. The comprehensive measurements from the Van Allen Probes sensors (MagEIS and REPT) allow us to examine more thoroughly such spectral properties throughout the course of both enhancement and depletion events.

Figure 10 shows composite energy spectra at L = 4.5 beginning on 9 September before the outer belt depletion all the way through to after the restoration of the relativistic population on 27 September. We see from the high-resolution spectral data that the energy distributions cannot typically be described as simple power laws. Instead, during times of active solar wind forcing (12–14 September and 19–21 September) the spectrum is better described as an exponential ($j = j_0 e^{-E/E_0}$) spectrum. During the times of relativistic electron enhancement (9–10 September and 21–23 September) the spectrum is quite remarkable with a broad, almost flat characteristic from below $E \sim 100$ keV all the way to $E \sim 1.0$ MeV. Only above $E = 1$ MeV are the electron fluxes elevated.

After the relativistic electron dropout during the 12 September storm, the tens of keV source population continues to decline, yet the hundreds of keV seed population remains elevated until a dramatic drop on 17 September, as was noted earlier. From 19 September onward, when the high-speed stream reaches the magnetosphere, the seed population remains high, then drops, then regains higher flux levels after 25 September. In this way, the behavior of the seed energies is very similar between the 12 September and the 19 September storms. However, the behavior of the source population at the lowest energy range is very different over the two events. The tens of keV source energy electrons show essentially no change from 19 September through 27 September. With the source population level remaining high, the chorus waves are able to grow and, over time, accelerate the seed population to the MeV energies that are seen returning after 22 September. This novel look at the high-resolution energy spectrum in the outer radiation belt presents the picture of three distinct electron populations; a departure from the previous portrayal of two power law spectra that join in the hundreds of keV region. Careful observation reveals a full radiation belt electron spectrum that often shows a plateau in the middle-energy regime and revolves or rocks around 600–700 keV throughout varying solar wind and geomagnetic activity.

7. Discussion and Conclusions

Early research discussed previously in this paper established that a prevalent pattern of solar wind-magnetosphere coupling occurs during strong solar wind forcing events. In this pattern, high solar wind speed leads to strong substorm activity and from this there emerges a source/seed population of electrons that ordinarily is further processed within the magnetosphere to produce a relativistic electron population throughout much of the outer radiation zone. This sequence occurs commonly enough that linear prediction filter analysis has
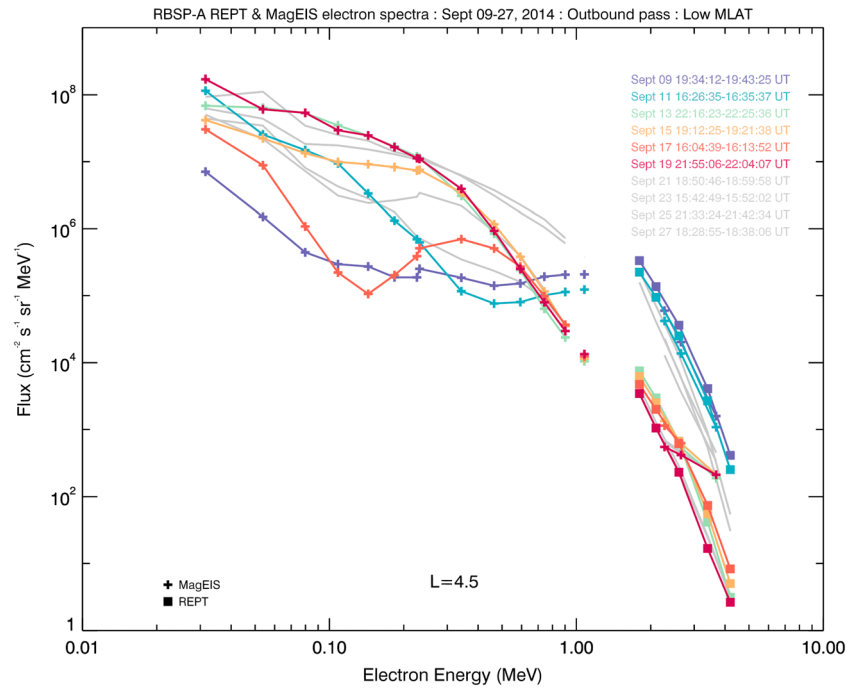
Figure 10. Evolution of energy spectrum across MagEIS and REPT energies: 9–27 September. The gap in the energy spectra from >1 MeV to ~2.5 MeV is due to missing MagEIS data channels over this full event period. All spectra are taken from outbound passes at magnetic latitude ≤ ~5°.

revealed the "transfer function" between solar wind drivers and radiation belt responses [*Baker et al.*, 1990]. By convolving the prediction filter response function with the measured upstream solar wind speed, for example, the linear prediction filter can provide a several day forecast of expected relativistic electron fluxes at GEO, based on the *Baker et al.* [1990] analysis. This work has formed the basis for the Relativistic Electron Forecast Model that has, for many years, been operational at the Space Weather Prediction Center of NOAA in Boulder, Colorado (www.swpc.noaa.gov/products/relativistic-electron-forecast-model).

As was noted previously, however, statistical studies of the relationship of solar wind speed and total electron radiation belt content [*Baker et al.*, 2004] or GEO relativistic electron fluxes [*Reeves et al.*, 2011; *Li et al.*, 2011] show that there can be very high radiation belt particle fluxes even when concurrent solar wind speeds are quite low. Thus, there is tremendous scatter in the data. What is demonstrably true is that relativistic electron fluxes in the outer Van Allen belt only seldom are low when the solar wind speed is high; thus, a triangular distribution pattern is found for the scatterplots of flux and its moments (number and energy density and temperature) versus solar wind speed [*Baker et al.*, 2004; *Reeves et al.*, 2011; *Hartley et al.*, 2014]: High fluxes at low solar wind speeds are common, but there are few cases of low fluxes (or low number and energy densities) at high solar wind speeds.

The work presented here shows that at least some of the time, the above pattern is violated. When the IMF is northward during and after a high-speed solar wind stream period, the outer zone electron flux level can be quite low throughout the stream period. From the statistical studies cited above, such events must be relatively rare. In most cases of high-speed streams, there must be enough southward IMF to produce substorm injections of source and seed electrons.

The results presented in this paper make it quite clear that the radiation belt accelerator is a rather finely tuned "machine." If the IMF does not have a southward component during an episode of high solar wind flow speed, then magnetospheric substorm activity does not occur. Without substorms, there is no injection of hot plasma and energetic electrons into the region 5 ≤ L ≤ 7. Without the source particles (up to tens of keV energy) the lower band chorus waves are not produced (amplified). Without chorus waves—even if there are residual seed population electrons—there is not an effective acceleration event for multi-MeV electrons in the outer zone. Moreover, not all substorms are capable of initiating this process. For example, the particle

injections on 16 September, mentioned earlier as ending a 3 day period of decreasing fluxes, injected a source population over a limited L range and lacked a substantially enhanced seed population; the injections were only prominent in the 30–100 keV fluxes at GOES 13 (Figure 2) and did not extend inward of L = 5.5–6 (Figure 4). In contrast, the injections on 22 September had a large >100 keV component at GOES 13 (Figure 2) and were associated with a large increase in MagEIS 30 keV fluxes nearly to L = 4 (Figure 4) and with an increase in $E > 2$ MeV fluxes above the GOES instrument backgrounds.

This paper has also addressed to some extent the questions surrounding the role of ULF waves in the acceleration, transport, and loss of relativistic electrons in the outer zone. As shown, for example, by *Rostoker et al.* [1998], ULF wave power enhancements often are associated with relativistic electron outer belt flux increases. In this paper, we have confirmed such an association throughout the outer radiation zone. It appears that ULF waves play two key roles: (1) enhanced outward diffusion of electrons toward the magnetopause to help drive radiation belt depletion and (2) enhanced inward radial diffusion of mildly relativistic electrons (1–2 MeV) to pump up electrons to multi-MeV energies in the trailing part of high-speed solar wind streams. However, the full significance of ULF involvement in the process detailed here is not entirely clear, and further study is planned to evaluate the role of ULF waves in this time period, and other analogous events.

References

Baker, D. N., P. R. Higbie, R. D. Belian, and E. W. Hones Jr. (1979), Do Jovian electrons influence the terrestrial outer radiation zone?, *Geophys. Res. Lett.*, 6, 531–534, doi:10.1029/GL006i006p00531.

Baker, D. N., J. B. Blake, R. W. Klebesadel, and P. R. Higbie (1986), Highly relativistic electrons in the Earth's outer magnetosphere, I. Lifetimes and temporal history 1979–1984, *J. Geophys. Res.*, 91, 4265–4276, doi:10.1029/JA091iA04p04265.

Baker, D. N., R. L. McPherron, T. E. Cayton, and R. W. Klebesadel (1990), Linear prediction filter analysis of relativistic electron properties at 6.6 R_E, *J. Geophys. Res.*, 95, 15,133–15,140, doi:10.1029/JA095iA09p15133.

Baker, D. N., T. I. Pulkkinen, V. Angelopoulos, W. Baumjohann, and R. L. McPherron (1996), The neutral line model of substorms: Past results and present view, *J. Geophys. Res.*, 101(12), 995–13,010, doi:10.1029/95JA03753.

Baker, D. N., et al. (1997), Recurrent geomagnetic storms and relativistic electron enhancements in the outer magnetosphere: ISTP coordinated measurements, *J. Geophys. Res.*, 102, 14,141–14,148, doi:10.1029/97JA00565.

Baker, D. N., S. G. Kanekal, and J. B. Blake (2004), Characterizing the Earth's outer Van Allen zone using the Radiation Belt Content (RBC) index, *Space Weather*, 2, S02003, doi:10.1029/2003SW000026.

Baker, D. N., et al. (2012), The Relativistic Electron-Proton Telescope (REPT) instrument on board the Radiation Belt Storm Probes (RBSP) spacecraft: Characterization of Earth's radiation belt high-energy particle populations, *Space Sci. Rev.*, doi:10.1007/s11214-012-9950-9.

Baker, D. N., et al. (2013), A long-lived relativistic electron storage ring embedded within the Earth's outer Van Allen radiation zone, *Science*, 340(6129), 186–190, doi:10.1126/science.1233518.

Baker, D. N., et al. (2014a), An impenetrable barrier to ultra-relativistic electrons in the Van Allen radiation belt, *Nature*, 515, 531–534, doi:10.1038/nature13956.

Baker, D. N., et al. (2014b), Gradual diffusion and punctuated phase space density enhancements of highly relativistic electrons: Van Allen Probes observations, *Geophys. Res. Lett.*, 41, 1351–1358, doi:10.1002/2013GL058942.

Blake, J. B., D. N. Baker, N. Turner, K. W. Ogilvie, and R. P. Lepping (1997), Correlation of changes in the outer-zone relativistic electron population with upstream solar wind and magnetic field measurements, *Geophys. Res. Lett.*, 24, 927–929, doi:10.1029/97GL00859.

Blake, J. B., et al. (2013), The Magnetic Electron Ion Spectrometer (MagEIS) instruments aboard the Radiation Belt Storm Probes (RBSP) spacecraft, *Space Sci. Rev.*, doi:10.1007/s11214-013-9991-8.

Boyd, A. J., H. E. Spence, S. G. Claudepierre, J. F. Fennell, J. B. Blake, D. N. Baker, G. D. Reeves, D. L. Turner, and H. O. Funsten (2014), Quantifying the radiation belt seed population in the 17 March 2013 electron acceleration event, *Geophys. Res. Lett.*, 41, 2275–2281, doi:10.1002/2014GL059626.

Chen, Y., R. H. W. Friedel, and G. D. Reeves (2006), Phase space density distributions of energetic electrons in the outer radiation belt during two Geospace Environment Modeling Inner Magnetosphere/Storms selected storms, *J. Geophys. Res.*, 111, A11S04, doi:10.1029/2006JA011703.

Claudepierre, S. G., S. R. Elkington, and M. Wiltberger (2008), Solar wind driving of magnetospheric ULF waves: Pulsations driven by velocity shear at the magnetopause, *J. Geophys. Res.*, 113, A05218, doi:10.1029/2007JA012890.

Elkington, S. R., A. A. Chan, and M. Wiltberger (2012), Global structure of ULF waves during the 24–26 September 1998 geomagnetic storm, in *Dynamics of the Earth's Radiation Belts and Inner Magnetosphere*, edited by D. Summers et al., AGU, Washington, D. C., doi:10.1029/2012GM001348.

Fennell, J. F., S. G. Claudepierre, J. B. Blake, T. P. O'Brien, J. H. Clemmons, D. N. Baker, H. E. Spence, and G. D. Reeves (2015), Van Allen Probes show the inner radiation zone contains no MeV electrons: ECT/MagEIS data, *Geophys. Res. Lett.*, 42, 1283–1289, doi:10.1002/2014GL062874.

Foster, J. C., et al. (2014), Prompt energization of relativistic and highly relativistic electrons during substorm intervals: Van Allen Probes observation, *Geophys. Res. Lett.*, 41, 20–25, doi:10.1002/2013GL058438.

Funsten, H. O., et al. (2013), Helium, Oxygen, Proton, and Electron (HOPE) mass spectrometer for the Radiation Belt Storm Probes mission, *Space Sci. Rev.*, doi:10.1007/s11214-013-9968-7.

Green, J. C., and M. G. Kivelson (2004), Relativistic electrons in the outer radiation belt: Differentiating between acceleration mechanisms, *J. Geophys. Res.*, 109, A03213, doi:10.1029/2003JA010153.

Green, J. C., T. G. Onsager, T. P. O'Brien, and D. N. Baker (2004), Testing loss mechanisms capable of rapidly depleting relativistic electron flux in the Earth's outer radiation belt, *J. Geophys. Res.*, 109, A12211, doi:10.1029/2004JA010579.

Hajra, R., et al. (2015), Relativistic (E > 0.6, >2.0, and >4.0 MeV) electron acceleration at geosynchronous orbit during high-intensity, long duration, continuous AE activity (HILDCAA) events, *Astrophys. J.*, *799*, 39, doi:10.1088/0004-637X/799/1/39.

Hanser, F. A. (2011), EPS/HEPAD calibration and data handbook, Tech. Rep. GOESN-ENG-048D, Assurance Technol. Corp., Carlisle, Mass.

Hartley, D. P., M. H. Denton, J. C. Green, T. G. Onsager, J. V. Rodriguez, and H. J. Singer (2013), Case studies of the impact of high-speed solar wind streams on the electron radiation belt at geosynchronous orbit: Flux, magnetic field, and phase space density, *J. Geophys. Res. Space Physics*, *118*, 6964–6979, doi:10.1002/2013JA018923.

Hartley, D. P., M. H. Denton, and J. V. Rodriguez (2014), Electron number density, temperature, and energy density at GEO and links to the solar wind: A simple predictive capability, *J. Geophys. Res. Space Physics*, *119*, 4556–4571, doi:10.1002/2014JA019779.

Hietala, H., E. K. J. Kilpua, D. L. Turner, and V. Angelopoulos (2014), Depleting effects of ICME-driven sheath regions on the outer electron radiation belt, *Geophys. Res. Lett.*, *41*, 2258–2265, doi:10.1002/2014GL059551.

Horne, R. B., R. M. Thorne, S. A. Glauert, J. M. Albert, N. P. Meredith, and R. R. Anderson (2005), Timescale for radiation belt electron acceleration by whistler mode chorus waves, *J. Geophys. Res.*, *110*, A03225, doi:10.1029/2004JA010811.

Hudson, M. K., S. R. Elkington, J. G. Lyon, V. A. Marchenko, I. Roth, M. Temerin, J. B. Blake, M. S. Gussenhoven, and J. R. Wygant (1997), Simulations of radiation belt formation during storm sudden commencements, *J. Geophys. Res.*, *102*, 14,087–14,102, doi:10.1029/97JA03995.

Hudson, M. K., B. T. Kress, H.-R. Mueller, J. A. Zastrow, and J. Bernard Blake (2008), Relationship of the Van Allen radiation belts to solar wind drivers, *J. Atmos. Sol. Terr. Phys.*, *70*(5), 708–729, doi:10.1016/j.jastp.2007.11.003.

Kanekal, S. G., D. N. Baker, J. B. Blake, B. Klecker, R. A. Mewaldt, and G. M. Mason (1999), Magnetospheric response to magnetic cloud (coronal mass ejection) events: Relativistic electron observations from SAMPEX and Polar, *J. Geophys. Res.*, *104*(A11), 24,885–24,894, doi:10.1029/1999JA900239.

Kletzing, C. A., et al. (2013), The Electric and Magnetic Field Instrument and Suite and Integrated Science (EMFISIS) on RBSP, *Space Sci. Rev.*, *179*, 127–181.

Li, W., B. Ni, R. M. Thorne, J. Bortnik, J. C. Green, C. A. Kletzing, W. S. Kurth, and G. B. Hospodarsky (2013), Constructing the global distribution of chorus wave intensity using measurements of electrons by the POES satellites and waves by the Van Allen Probes, *Geophys. Res. Lett.*, *40*, 4526–4532, doi:10.1002/grl.50920.

Li, W., et al. (2014), Radiation belt electron acceleration by chorus waves during the 17 March 2013 storm, *J. Geophys. Res. Space Physics*, *119*, 4681–4693, doi:10.1002/2014JA019945.

Li, X., M. Temerin, D. N. Baker, and G. D. Reeves (2011), Behavior of MeV electrons at geosynchronous orbit during last two solar cycles, *J. Geophys. Res.*, *116*, A11207, doi:10.1029/2011JA016934.

Li, X., R. S. Selesnick, D. N. Baker, A. N. Jaynes, S. G. Kanekal, Q. G. Schiller, and L. W. Blum (2015), Upper limit on the inner radiation belt MeV electron intensity, *J. Geophys. Res. Space Physics*, *120*, 1215–1228, doi:10.1002/2014JA020777.

Luo, B., X. Li, M. Temerin, and S. Liu (2013), Prediction of the *AU*, *AL*, and *AE* indices using solar wind parameters, *J. Geophys. Res. Space Physics*, *118*, 7683–7694, doi:10.1002/2013JA019188.

McIlwain, C. E. (1966), Magnetic coordinates, *Space Sci. Rev.*, *5*, 585–598.

McPherron, R. L., C. T. Russell, and M. P. Aubry (1973), Satellite studies of magnetospheric substorms on August 15, 1968, 9, phenomenological model for substorms, *J. Geophys. Res.*, *78*, 3131–3149, doi:10.1029/JA078i016p03131.

Miyoshi, Y., and R. Kataoka (2008), Flux enhancement of the outer radiation belt electrons after the arrival of stream interaction regions, *J. Geophys. Res.*, *113*, A03209, doi:10.1029/2007JA012506.

Onsager, T. G., R. Grubb, J. Kunches, L. Matheson, D. Speich, R. Zwickl, and H. Sauer (1996), Operational uses of the GOES energetic particle detectors, in *GOES-8 and Beyond: 7–9 August 1996, Denver, Colorado, Proc. SPIE Int. Soc. Opt. Eng.*, vol. 2812, edited by E. R. Washwell, 281 pp., Bellingham, Wash.

Onsager, T. G., G. Rostoker, H.-J. Kim, G. D. Reeves, T. Obara, H. J. Singer, and C. Smithtro (2002), Radiation belt electron flux dropouts: Local time, radial, and particle-energy dependence, *J. Geophys. Res.*, *107*(A11), 1382, doi:10.1029/2001JA000187.

Onsager, T. G., J. C. Green, G. D. Reeves, and H. J. Singer (2007), Solar wind and magnetospheric conditions leading to the abrupt loss of outer radiation belt electrons, *J. Geophys. Res.*, *112*, A01202, doi:10.1029/2006JA011708.

Paulikas, G. A. and Blake, J. B. (1979), Effects of the solar wind on magnetospheric dynamics: Energetic electrons at the synchronous orbit, in *Quantitative Modeling of Magnetospheric Processes*, edited by W. P. Olson, AGU, Washington, D. C., doi:10.1029/GM021p0180.

Reeves, G. D., K. L. McAdams, R. H. W. Friedel, and T. P. O'Brien (2003), Acceleration and loss of relativistic electrons during geomagnetic storms, *Geophys. Res. Lett.*, *30*(10), 1529, doi:10.1029/2002GL016513.

Reeves, G. D., et al. (2011), On the relationship between relativistic electron flux and solar wind velocity: Paulikas and Blake revisited, *J. Geophys. Res.*, *116*, A02213, doi:10.1029/2010JA015735.

Reeves, G. D., et al. (2013), Electron acceleration in the heart of the Van Allen radiation belts, *Science*, *341*(6149), 991–994, doi:10.1126/science.1237743.

Rodriguez, J. V. (2014), GOES EPEAD science-quality electron fluxes algorithm theoretical basis document, NOAA Nat. Geophys. Data Center.

Rostoker, G., S. Skone, and D. N. Baker (1998), On the origin of relativistic electrons in the magnetosphere associated with some geomagnetic storms, *Geophys. Res. Lett.*, *25*, 3701–3704, doi:10.1029/98GL02801.

Rufenach, C. L., R. F. Martin Jr., and H. H. Sauer (1989), A study of geosynchronous magnetopause crossings, *J. Geophys. Res.*, *94*(A11), 15,125–15,134, doi:10.1029/JA094iA11p15125.

Sergeev, V. A., et al. (2015), Event study combining magnetospheric and ionospheric perspectives of the substorm current wedge modeling, *J. Geophys. Res. Space Physics*, *119*, 9714–9728, doi:10.1029/2014JA020522.

Shue, J.-H., et al. (1998), Magnetopause location under extreme solar wind conditions, *J. Geophys. Res.*, *103*(A8), 17,691–17,700, doi:10.1029/98JA01103.

Singer, H. J., L. Matheson, R. Grubb, A. Newman, and S. D. Bouwer (1996), Monitoring space weather with the GOES magnetometers, in *SPIE Conference Proceedings*, *GOES-8 and Beyond*, vol. 2812, edited by E. R. Washwell, pp. 299-308, SPIE Int. Soc. Opt. Eng., Bellingham, Wash.

Spence, H. E., et al. (2013), Science goals and overview of the energetic particle, composition, and thermal plasma (ECT) suite on NASA's Radiation Belt Storm Probes (RBSP) mission, *Space Sci. Rev.*, doi:10.1007/s11214-013-0007-5.

Summers, D., C. Ma, N. P. Meredith, R. B. Horne, R. M. Thorne, D. Heynderickx, and R. R. Anderson (2002), Model of the energization of outer-zone electrons by whistler-mode chorus during the October 9, 1990 geomagnetic storm, *Geophys. Res. Lett.*, *29*(24), 2174, doi:10.1029/2002GL016039.

Summers, D., C. Ma, and T. Mukai (2004), Competition between acceleration and loss mechanisms of relativistic electrons during geomagnetic storms, *J. Geophys. Res.*, *109*, A04221, doi:10.1029/2004JA010437.

Summers, D., Tang, R. and Omura, Y. (2012), Linear and nonlinear growth of magnetospheric whistler mode waves, in *Dynamics of the Earth's Radiation Belts and Inner Magnetosphere*, edited by D. Summers et al., AGU, Washington, D. C., doi:10.1029/2012GM001298.

Temerin, M., and X. Li (2006), *Dst* model for 1995–2002, *J. Geophys. Res.*, *111*, A04221, doi:10.1029/2005JA011257.

Thorne, R. M., et al. (2013a), Evolution and slow decay of an unusual narrow ring of relativistic electrons near L~ 3.2 following the September 2012 magnetic storm, *Geophys. Res. Lett.*, *40*, 3507–3511, doi:10.1002/grl.50627.

Thorne, R. M., et al. (2013b), Rapid local acceleration of relativistic radiation belt electrons by magnetospheric chorus, *Nature*, *504*, 411–414, doi:10.1038/nature12889.

Tsurutani, B. T., W. D. Gonzalez, A. L. C. Gonzalez, F. Tang, J. K. Arballo, and M. Okada (1995), Interplanetary origin of geomagnetic activity in the declining phase of the solar cycle, *J. Geophys. Res.*, *100*, 21,717–21,733, doi:10.1029/95JA01476.

Tu, W., G. S. Cunningham, Y. Chen, S. K. Morley, G. D. Reeves, J. B. Blake, D. N. Baker, and H. Spence (2014), Event-specific chorus wave and electron seed population models in DREAM3D using the Van Allen Probes, *Geophys. Res. Lett.*, *41*, 1359–1366, doi:10.1002/2013GL058819.

Turner, D. L., et al. (2012), Explaining sudden losses of outer radiation belt electrons during geomagnetic storms, *Nat. Phys.*, *8*, 208–212, doi:10.1038/nphys2185.

Wilken, B., C. K. Goertz, D. N. Baker, P. R. Higbie, and T. A. Fritz (1982), The SSC on July 29, 1977 and its propagation within the magnetosphere, *J. Geophys. Res.*, *87*, 5901–5910, doi:10.1029/JA087iA08p05901.